Neoadjuvant Selicrelumab, an Agonist CD40 Antibody, Induces Changes in the Tumor Microenvironment in Patients with Resectable Pancreatic Cancer

Katelyn T. Byrne[1,2], Courtney B. Betts[3,4], Rosemarie Mick[1,5], Shamilene Sivagnanam[3], David L. Bajor[6], Daniel A. Laheru[7], E. Gabriela Chiorean[8], Mark H. O'Hara[1], Shannon M. Liudahl[3], Craig Newcomb[5], Cécile Alanio[2,9], Ana P. Ferreira[3], Byung S. Park[4], Takuya Ohtani[9], Austin P. Huffman[1], Sara A. Väyrynen[10], Andressa Dias Costa[10], Judith C. Kaiser[11], Andreanne M. Lacroix[11], Colleen Redlinger[1], Martin Stern[12], Jonathan A. Nowak[13], E. John Wherry[1,2,9], Martin A. Cheever[11], Brian M. Wolpin[10], Emma E. Furth[1], Elizabeth M. Jaffee[6], Lisa M. Coussens[3,4], and Robert H. Vonderheide[1,2]

ABSTRACT

Purpose: CD40 activation is a novel clinical opportunity for cancer immunotherapy. Despite numerous active clinical trials with agonistic CD40 monoclonal antibodies (mAb), biological effects and treatment-related modulation of the tumor microenvironment (TME) remain poorly understood.

Patients and Methods: Here, we performed a neoadjuvant clinical trial of agonistic CD40 mAb (selicrelumab) administered intravenously with or without chemotherapy to 16 patients with resectable pancreatic ductal adenocarcinoma (PDAC) before surgery followed by adjuvant chemotherapy and CD40 mAb.

Results: The toxicity profile was acceptable, and overall survival was 23.4 months (95% confidence interval, 18.0–28.8 months). Based on a novel multiplexed immunohistochemistry platform, we report evidence that neoadjuvant selicrelumab leads to major differences in the TME compared with resection specimens from treatment-naïve PDAC patients or patients given neoadjuvant chemotherapy/chemoradiotherapy only. For selicrelumab-treated tumors, 82% were T-cell enriched, compared with 37% of untreated tumors ($P = 0.004$) and 23% of chemotherapy/chemoradiation-treated tumors ($P = 0.012$). T cells in both the TME and circulation were more active and proliferative after selicrelumab. Tumor fibrosis was reduced, M2-like tumor-associated macrophages were fewer, and intratumoral dendritic cells were more mature. Inflammatory cytokines/sec CXCL10 and CCL22 increased systemically after selicrelumab.

Conclusions: This unparalleled examination of CD40 mAb therapeutic mechanisms in patients provides insights for design of subsequent clinical trials targeting CD40 in cancer.

Introduction

CD40 is a cell-surface member of the tumor necrosis factor superfamily of receptors that functions as a proximal regulator of myeloid cell function and adaptive immunity. Agonistic CD40 monoclonal antibodies (mAb) are under active clinical investigation as novel agents for immune activation and cancer immunotherapy, distinct from immune-checkpoint blockade (1). Mechanistically, and largely based on preclinical cancer models, agonistic CD40 mAb activates various effector functions in $CD40^+$ macrophages, B cells, and dendritic cells (DC)—mimicking CD40 cross-linking and activation by CD40 ligand (CD154) on $CD4^+$ T cells and driving antitumor $CD8^+$ T-cell immunity (2). In preclinical models, delivering agonist CD40 mAb activates DCs, induces Th1 cytokines such as IL12, and reeducates tumor-associated macrophages toward an M1-like phenotype with capacity to degrade tumor stroma (3, 4). As such, CD40 activation represents a unique pathway for bridging DC activation and adaptive immunity in cancer independently of innate immune receptors (5). CD40 mAbs synergize with chemotherapy and radiotherapy and sensitize tumors otherwise refractory to treatment with anti–CTLA-4 or anti–PD-1/PD-L1 mAb (6, 7). In particular, extensive studies in genetically engineered pancreatic cancer mouse models with low tumor mutational burden demonstrate that CD40 mAb in combination with chemotherapy renders tumors susceptible to T-cell–dependent destruction and potentiates durable remissions (4).

Multiple single-agent and combination studies of CD40 mAb in cancer have been developed around an emerging array of agonistic antibody formulations (1). Promising rates of objective clinical responses have been reported, and manageable and feasible outpatient

[1]Abramson Cancer Center, Perelman School of Medicine, University of Pennsylvania, Philadelphia, Pennsylvania. [2]Parker Institute for Cancer Immunotherapy, Perelman School of Medicine, University of Pennsylvania, Philadelphia, Pennsylvania. [3]Department of Cell, Developmental and Cancer Biology, Oregon Health and Science University, Portland, Oregon. [4]Knight Cancer Institute, Oregon Health and Science University-Portland State University School of Public Health, Portland, Oregon. [5]Department of Biostatistics, Epidemiology, and Informatics, Perelman School of Medicine, University of Pennsylvania, Philadelphia, Pennsylvania. [6]Case Comprehensive Cancer Center, Cleveland, Ohio. [7]Sidney Kimmel Comprehensive Cancer Center, Johns Hopkins University, Baltimore, Maryland. [8]University of Washington School of Medicine, Fred Hutchinson Cancer Research Center, Seattle, Washington. [9]Department of Systems Pharmacology and Translational Therapeutics, Institute for Immunology, Perelman School of Medicine, University of Pennsylvania, Philadelphia, Pennsylvania. [10]Department of Medical Oncology, Dana-Farber Cancer Institute, Harvard Medical School, Boston, Massachusetts. [11]Fred Hutchinson Cancer Research Center, Seattle, Washington. [12]Roche Pharma Research and Early Development, Roche Innovation Center, Zurich, Switzerland. [13]Department of Pathology, Brigham and Women's Hospital, Harvard Medical School, Boston, Massachusetts.

K.T. Byrne, C.B. Betts, and R. Mick contributed equally to this article.

Corresponding Author: Robert H. Vonderheide, Abramson Cancer Center, University of Pennsylvania, 12-114 South Paviliion, Philadelphia, PA19104. E-mail: rhv@upenn.edu

Clin Cancer Res 2021;27:4574–86

doi: 10.1158/1078-0432.CCR-21-1047

Translational Relevance

Pancreatic ductal adenocarcinoma (PDAC) is a highly treatment-refractory disease, with fewer than 1% of patients responding to current immunotherapeutic interventions, highlighting the need for novel approaches for improved clinical outcomes. Here we report for the first time in humans an in-depth analysis of the tumor site after neoadjuvant agonistic CD40 monoclonal antibody (mAb) therapy. The PDAC tumor site after CD40 mAb displayed a T-cell–enriched phenotype with concomitant increases in dendritic cells and reeducated macrophages, and a depletion of tumor stroma. These alterations in the tumor site were associated with systemic T-cell activation and clonal expansion in the periphery. Together, these data provide novel, proof-of-concept evidence regarding the mechanisms of agonistic CD40 mAb use in the clinical setting and inform next-generation agonistic CD40 clinical trials, especially for patients with PDAC.

dosing schedules have been established for use in phase II studies. Toxicities have been mild to moderate, including transient cytokine release syndrome (CRS) and transient alterations in hematologic and liver function tests. Clinical data demonstrate potential efficacy of CD40 mAb and chemotherapy in patients with pancreatic ductal adenocarcinoma (PDAC; refs. 3, 8). In a phase Ib study of the CD40 mAb APX005M with gemcitabine and nab-paclitaxel with or without anti–PD-1 nivolumab, objective responses were observed in 58% of patients with newly diagnosed metastatic PDAC (9).

Biological effects of CD40 activation in patients—especially with respect to modulation of the tumor microenvironment (TME) and T-cell infiltration, as predicted in preclinical models—remain poorly understood because, to date, clinical trials with CD40 mAb have minimally studied patient tumor samples, hampered by poor yield and low cellularity common with such biopsy fragments. Here, we performed a clinical trial of the CD40 mAb selicrelumab (10, 11) with or without chemotherapy given in both the neoadjuvant and adjuvant settings for patients with resectable PDAC. Application of a curated antibody panel by multiplexed IHC (mIHC) on resection samples revealed major alterations in the TME of patients receiving selicrelumab compared with samples from therapy-naïve control PDAC patients (12). Marked T-cell infiltration in the TME after selicrelumab was associated with loss of stroma, systemic inflammation, and T-cell activation. This study provides proof-of-concept regarding the mechanisms of agonistic CD40 mAb in cancer and informs the design of next-generation CD40 mAb clinical trials.

Patients and Methods

Human subjects

An open-label, phase I clinical trial (Cancer Immunotherapy Trials Network CITN11-01; NCT02588443) at four sites in the United States was conducted to determine if adding the agonist anti-CD40 fully human IgG2 mAb selicrelumab (RG7876, previously known as CP-870,893; ref. 10) to a standard chemotherapy regimen of gemcitabine and nab-paclitaxel both before and after surgery was feasible, safe and beneficial to patients with resectable PDAC. Primary objectives were to determine the feasibility and safety, and secondary objectives were to estimate disease-free survival (DFS) and overall survival (OS), and to assess immune biomarkers in blood and surgical specimens. The trial was approved by each site's Institutional Review Board (IRB) and FDA (IND 126456, held by the investigator), and studies were conducted in accordance with the ethical guidelines outlined in the Declaration of Helsinki. Details of trial design, conduct, and endpoints are provided in Supplementary Data and Methods.

Surgical resection specimens from contemporary treatment-naïve patients or patients treated with neoadjuvant chemotherapy/chemoradiotherapy were obtained with site IRB approval and written informed consent from the patients at the University of Pennsylvania, Dana-Farber Cancer Institute/Brigham and Women's Hospital, and the Oregon Health and Science University (12). Peripheral blood from normal donors was obtained after written informed consent with University of Pennsylvania IRB approval.

Analysis of surgical specimens

Formalin-fixed, paraffin-embedded (FFPE) surgical tissue samples were assessed using hematoxylin and eosin and Masson's trichrome staining. Stained slides were digitally scanned (Leica Biosystems) and svs files imported into QuPath (13). The tumor bed was annotated and the percentage of fibrosis was determined using a pixel classifier. Chromogen-based mIHC was performed as previously described (14–17), having been adapted for PDAC and reported recently (12). Further details regarding assessment of the immune contexture, region-of-interest (ROI) selection, image processing, and single-cell and other analyses are provided in Supplementary Data and Methods.

Tumors from this clinical trial also underwent DNA sequencing for mutational profiling (Tempus Corporation), as well as T-cell receptor beta (TCRβ) deep sequencing (Adaptive Biotechnologies). Details of sample preparation, processing, and assessment are provided in Supplementary Data and Methods.

Analysis of blood-based biomarkers

Serum and peripheral blood mononuclear cells (PBMC) obtained at baseline and serially after treatment and surgery were analyzed with a panel of assays, including cytokine quantification (Luminex, R&D Systems), mass cytometry (CyTOF), and T-cell receptor deep sequencing (Adaptive Biotechnologies). Details of sample preparation, processing, and assessment are provided in Supplementary Data and Methods.

Statistical analysis

For the clinical trial, baseline demographics and the clinical outcomes were summarized with descriptive statistics. To assess the hypothesis that the feasibility rate was 50%, the binomial probability of the observed feasibility rate was computed by combining the two arms, as described in Supplementary Data and Methods. For DFS and OS, median and 95% confidence intervals plus 1-year rates $\pm$ SE were estimated by the Kaplan–Meier method. The degree of intratumoral fibrosis was compared between experimental and untreated samples by the Mann–Whitney rank test. Statistical considerations for mIHC analysis have been recently reported (12). For global TME analyses, a linear mixed-effect model was used, with treatment group as between-group factor and ROI location as within-group factor. Prior to applying the mixed-effect model, the data were transformed using logarithmic function with base 10. The Bayesian Information Criteria was used to assess within subject covariance structure. The Tukey multiple comparison correction was used to control overall type I error. Differences in TME cluster types between experimental and untreated samples were tested with Fisher exact test (2×3 contingency table). For intratumoral analyses, Kruskal–Wallis nonparametric one-way ANOVA was used with Dunn multiple comparisons correction.

Table 1. Baseline demographic and clinical characteristics of treated patients.

Characteristic	Arm I neoadjuvant selicrelumab *N* = 11	Arm II neoadjuvant nab-paclitaxel + gemcitabine + selicrelumab *N* = 5	Total *N* = 16
Age at diagnosis, years			
Mean ± SD	56.5 ± 8.5	64.2 ± 6.4	59.0 ± 8.5
Median (range)	54 (44–72)	63 (55–72)	56 (44–72)
Gender, *n* (%)			
Male	6 (54.6%)	4 (80.0%)	10 (62.5%)
Female	5 (45.4%)	1 (20.0%)	6 (37.5%)
Race/ethnicity, *n* (%)			
White	11 (100%)	4 (80.0%)	15 (93.8%)
Hispanic	0 (0.0%)	1 (20.0%)	1 (6.2%)
ECOG performance status, *n* (%)			
0, normal activity	9 (81.8%)	3 (60.0%)	12 (75.0%)
1, restricted activity	2 (18.2%)	2 (40.0%)	4 (25.0%)
Days since cancer diagnosis			
Mean ± SD	21.8 ± 12.3	30.2 ± 14.2	24.4 ± 13.0
Median (range)	22 (7–50)	26 (14–46)	23 (7–50)
CA19-9 level (U/mL)			
Mean ± SD	376.4 ± 759.1	897.0 ± 1,580.2	525.1 ± 1,017.2
Median (range)	106.3 (1.2–2,470.8)	159.5 (7.0–3,261.8)	106.3 (1.2–3,261.8)

The Wilcoxon matched-pair signed-rank test was used to assess paired differences (i.e., change from baseline, protocol day 0; to day 5 after selicrelumab, protocol day 8) measured by mass cytometry or cytokine quantification. Statistical analyses were performed using STATA v.16 (StataCorp), IBM SPSS v.26, or GraphPad Prism v7 (GraphPad Prism Software, Inc.). $P < 0.05$ was considered statistically significant.

Results

Clinical trial of agonist CD40 mAb selicrelumab with chemotherapy in patients with resectable PDAC

Sixteen patients with resectable PDAC initiated neoadjuvant therapy with either (i) selicrelumab (0.2 mg/kg i.v.) two weeks prior to surgery (arm I, $n = 11$) or (ii) gemcitabine (1,000 mg/m^2 i.v.) and nab-paclitaxel (125 mg/m^2 i.v.) followed 2 days later by selicrelumab prior to surgery (arm II, $n = 5$; **Table 1**). The CONSORT diagram for screening and enrollment is provided (Supplementary Fig. S1). Enrollment to arm II was allowed when safety was established for arm I, as detailed in Supplementary Data and Methods. Thirteen patients (9 on arm I and 4 on arm II) were able to initiate adjuvant therapy with gemcitabine/nab-paclitaxel followed by selicrelumab with up to four 28-day cycles (gemcitabine 1,000 mg/m^2 i.v. on days 1, 8, 15; nab-paclitaxel 125 mg/m^2 i.v. on days 1, 8, 15; selicrelumab 0.2 mg/kg i.v. on day 3). The sequence of chemotherapy and selicrelumab was based on preclinical (4, 18) and clinical studies (19). Arm II was closed to enrollment short of goal when no new patient was enrolled for a year. Based on DNA sequencing, the mutational profile of the resected tumors represented a typical picture of PDAC with frequent KRAS mutations and common mutations in TP53 and CDKN2A; one tumor had a pathologic mutation in BRCA2; no patient's tumor met the definition of MSI-high.

Adverse events (AE) attributed to selicrelumab neoadjuvant therapy were mostly mild. CRS with transient chills, fever, or rigor occurred in 10 of 16 patients, of which 9 were grade 1 (Supplementary Table S1). There was a single occurrence each of grade 3 hyperglycemia and elevated liver function tests (AST and ALT). Grade 2 AE included diarrhea, fatigue, headache, hypertension rash, and rigors. There were no serious adverse events (SAE) with neoadjuvant therapy. AEs attributed to selicrelumab adjuvant therapy were grade 3 fatigue (2 patients), hypertension, elevated AST/ALT, and thrombocytopenia (1 patient each); and grade 4 pancreatitis (1 patient; Supplementary Table S1). Six patients experienced grade 2 CRS. There were three SAEs in two patients: elevated AST/ALT and pancreatitis in a single patient attributed to selicrelumab, and fever in a second patient attributed to both selicrelumab and chemotherapy. Chemotherapy-related toxicities are detailed in Supplementary Table S2 and were all expected.

The median DFS was 13.8 months (95% CI, 2.9–24.8 months) for 15 patients who underwent surgery on the trial. The median DFS for arm I ($n = 11$) was 9.8 months (95% CI, 0.4–19.2 months) and the median for arm II ($n = 4$) had not been reached (**Fig. 1A**). The 1-year DFS rate ± SE was 49.9% ± 16.4% and 75.0% ± 21.7% on arms I and II, respectively. The median OS from surgery was 23.4 months (95% CI, 18.0–28.8). The median OS for arm I was 23.4 months (95% CI, 9.1–37.6 months) and the median had not been reached for arm II (**Fig. 1B**). The 1-year OS rate ± SE was 81.8% ± 11.8% and 100% on arms I and II, respectively. At either last contact or the time of database lock (i.e., May 10, 2019), 8 patients were alive at a median of 20.0 months after surgery (follow-up range, 12.2–34.8 months). Survival estimates were imprecise due to small sample sizes, but these survival rates are on par with a cohort of patients receiving no neoadjuvant intervention or a cohort of patients receiving a neoadjuvant chemo- or chemoradiation therapy, as shown in **Fig. 1C** (12).

Modulation of TME with selicrelumab

To dissect the pharmacodynamic effects of selicrelumab on the TME at 12 days after CD40 administration (protocol day 15), resected tumors were examined by standard histopathology and Masson's trichrome staining to evaluate cellularity and desmoplasia. Most notably, the mean percentage of fibrosis in tumors from patients treated with selicrelumab alone was approximately half that observed

Figure 1.

Survival estimates for patients who underwent surgical resection and eligible for adjuvant therapy. **A,** DFS from day of surgery by treatment arm and (**B**) OS from day of surgery by treatment arm and combined arms. **C,** Table comparing DFS and OS for the selicrelumab-treated cohort to two published cohorts: an untreated cohort and a chemo/chemoradiation-treated cohort, as indicated.

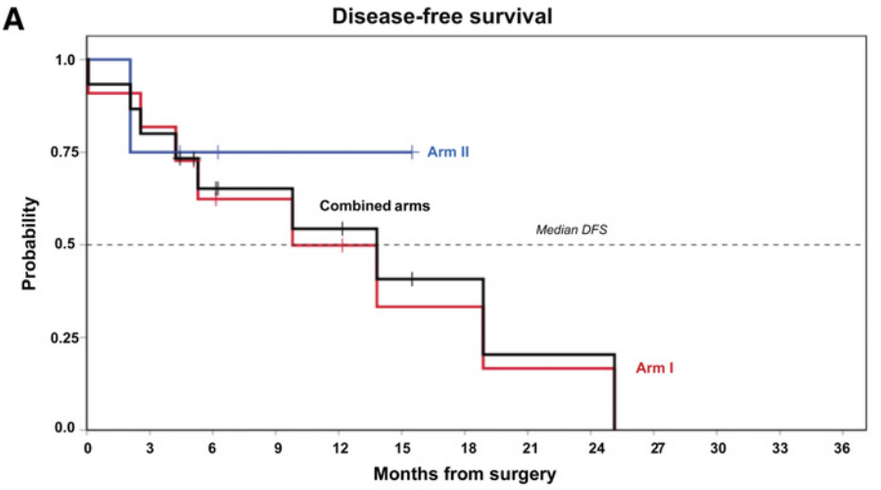

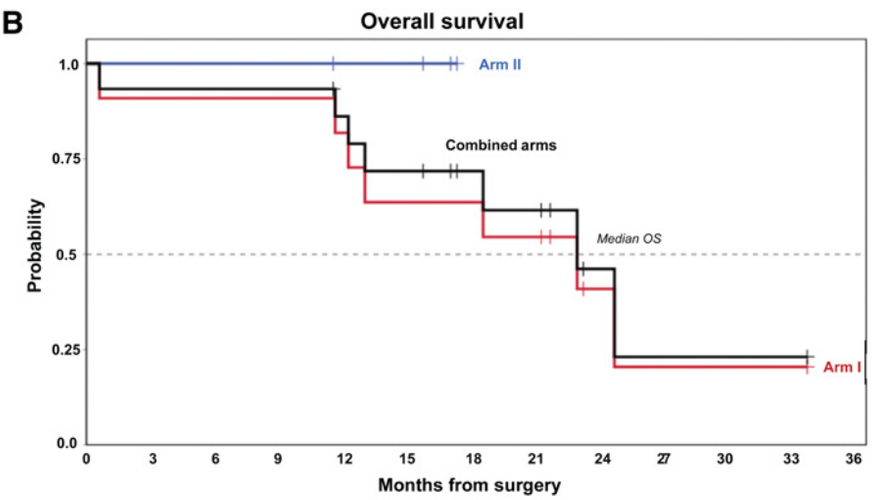

C

		DFS	OS
Selicrelumab cohort	Median	13.8 mos	23.4 mos
	95% CI	2.9–24.8 mos	18.0–28.8 mos
	Cohort size	15	15
Untreated cohort	Median	11.1 mos	20.6 mos
	95% CI	6.6–15.6 mos	16.4–24.8 mos
	Cohort size	100	104
Chemo/chemo-radiation cohort	Median	10.7 mos	20.5 mos
	95% CI	3.7–17.7 mos	15.4–25.6 mos
	Cohort size	11	13

in tumors from nine control patients (UPenn) who had undergone resection without neoadjuvant therapy ($P = 0.031$; illustrated in **Fig. 2A** and **B** and quantified in **Fig. 2C**).

Surgical samples were then evaluated with a mIHC platform (8 from arm I and 3 from arm II) to enable comprehensive assessment of immune contexture. This mIHC platform is a chromogen-based iterative staining method utilizing a curated panel of antibodies followed by a computational pipeline culminating in single-cell hierarchical gating to identify lymphoid and myeloid immune lineages, as described previously (15, 17) and summarized in Supplementary Fig. S2. Importantly, ROIs were selected following pathologic annotation and categorized as tumor (T), tumor adjacent stroma (TAS), adjacent normal pancreas tissue (AN), or tertiary lymphoid structure (TLS) ROIs. Further, the location of each ROI was recorded as related to the pathologists' tumor annotation (intratumoral, border, spanning, and distal) to allow for spatial characterization of immune infiltrates

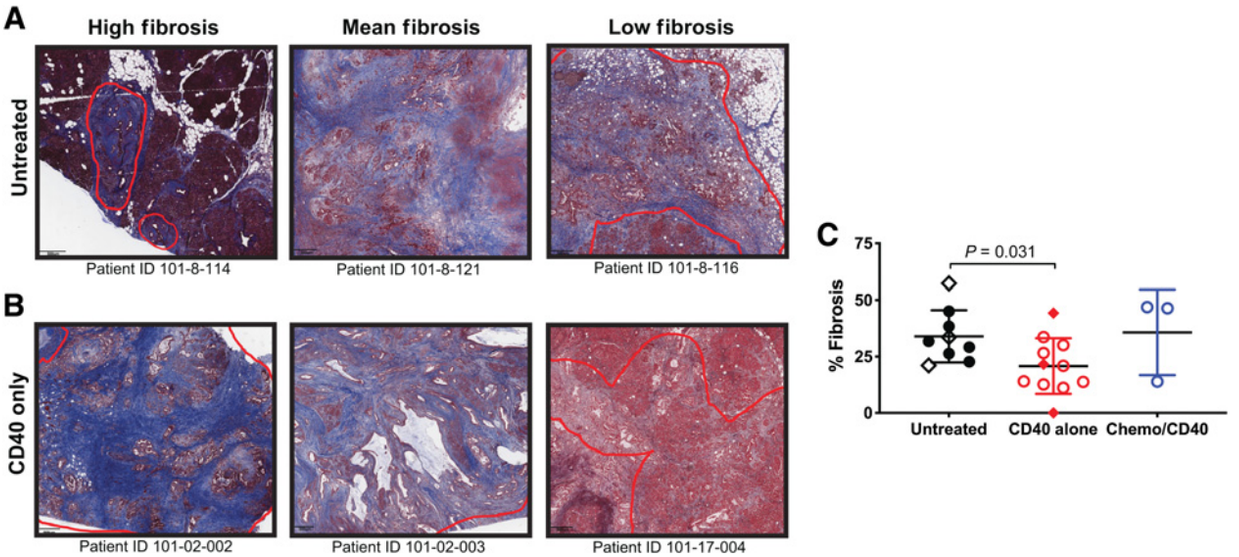

Figure 2.

Assessment of TME by histopathologic and IHC of the surgical resection specimen. Representative images of Mason's trichrome staining from (**A**) treatment-naïve cohort of UPenn patients or (**B**) patients treated with selicrelumab (arm I). Red lines indicate the border of tumor regions. **C,** Quantification of percent fibrosis in the TME for a set of untreated control PDAC resection samples and samples from arms I and II, as indicated. Each symbol represents a single patient, horizontal line indicates mean, and error bars indicate standard deviation from the mean (SD). Diamond symbols indicate representative image shown in **A** or **B**.

(defined in Supplementary Fig. S2, with ROI features summarized in Supplementary Table S3). A recent study by Liudahl and colleagues utilized mIHC to characterize PDAC immune ecosystems, a phenotypic and spatial immune atlas was constructed following assessment of 104 treatment-naïve and 13 neoadjuvant chemo/chemoradiation-treated PDAC resection samples (DFCI/BWH and OHSU, mean time to surgery after start of neoadjuvant therapy of 188 days), providing comparative analyses for our neoadjuvant study (12).

We then applied the immune atlas from Liudahl study to our patient samples. We first analyzed "globally" across the samples, and multiple ROI types (T, TAS, AN, and TLS) were quantitatively evaluated. Borderline statistical differences were revealed in total $CD45^+$ cell density ($P = 0.052$) across all ROI types (**Fig. 3A**, left), and neoplastic cell abundance ($P = 0.084$) within tumor ROIs (**Fig. 3A**, right) in selicrelumab-treated groups compared with the reference cohorts (Supplementary Table S4).

We next assessed how immune infiltrates were affected by either treatment (**Fig. 3B**) and/or spatial localization (**Fig. 3C**) and generated a statistical mixed-effects model to understand the two variables in combination (Supplementary Table S4). In terms of spatial localization in the TME, there were significant differences in total $CD45^+$ cell density regardless of the treatment group—greater in distal locations as compared with intratumoral ($P < 0.0001$), and greater in border locations compared with either intratumoral ($P < 0.0001$) or spanning regions ($P = 0.016$). This effect was linked to B cells, $CD4^+$ T cells, and $CD8^+$ T cells as these cell populations were largely excluded from intratumoral and spanning locations, whereas myeloid cells (including monocytes/macrophages or neutrophils/eosinophils) were not differentially distributed by spatial location (**Fig. 3B** and **C**; Supplementary Table S4). Statistically significant treatment effects were observed overall for densities of mature DC, $CD4^+$ T cells, and $CD8^+$ T cells (**Fig. 3B**; Supplementary Table S3). Mature DC density was greater in selicrelumab-treated tumors compared with either untreated tumors ($P < 0.001$) or chemo/chemoradiation-treated tumors ($P < 0.001$). $CD4^+$ T-cell density was similarly greater in both selicrelumab or selicrelumab/chemotherapy tumors compared with either untreated tumors or chemo/chemoradiation-treated tumors (adjusted P values shown in Supplementary Table S4, ranging from 0.003 to 0.015)—an effect appreciated in every spatial location (**Fig. 3C**). Treatment effects on $CD8^+$ cell density were most notable in comparing chemo/chemoradiation to selicrelumab/chemotherapy-treated tumors that approached statistical significance, and was best appreciated in distal and border areas rather than spanning or intratumoral areas (**Fig. 3C**). Of all ROI locations and treatments examined, the highest density of $CD4^+$ and $CD8^+$ T cells was observed in the distal region of selicrelumab and border region of selicrelumab/chemotherapy-treated tumors.

To understand leukocyte identity in closest proximity to neoplastic cells, we then applied unsupervised hierarchical clustering on histopathologically defined tumor regions studied from all patients and treatment groups ($N = 128$ total samples). Three unique clusters based on the dominant immune infiltrates emerged: granulocyte-enriched (22% of samples, 28/128), T-cell–enriched (39%, 50/128) and myeloid-enriched (39%, 50/128; **Fig. 3D**; Supplementary Fig. S3). Analysis of the cluster groups revealed that the T-cell–enriched cluster contained significantly reduced granulocytes and significantly greater abundance of total $CD4^+$ T cells than the other clusters (**Fig. 3E**). For 11 tumors resected after selicrelumab, 82% (9/11) were T-cell–enriched, compared with 37% (38/104) of untreated tumors ($P = 0.004$) and 23% (3/13) of chemotherapy/chemoradiation-treated tumors ($P = 0.012$). One selicrelumab-treated tumor from arm I was granulocytic-enriched and one was myeloid-enriched. Thus, tumors from patients treated with selicrelumab prior to surgery, with or without chemotherapy, were more likely to be classified as T-cell–enriched PDAC than untreated tumors or those treated with chemotherapy/chemoradiotherapy.

We then further focused on immune infiltrates within pathologically defined tumor ROIs and compared directly across treatment

groups (**Fig. 3F** and **G**; Supplementary Fig. S3). $CD4^+$ T cells were increased in abundance in both selicrelumab groups when compared with untreated or chemo/chemoradiation groups, and nearly reached statistical significance, as did the ratios of mature/immature DCs and $CD8^+$ T cells/$CD68^+$ monocytes/macrophages (**Fig. 3F**; Supplementary Fig. S3B). To measure monocyte/macrophage effector phenotype reflecting alternatively activated M2-like status, we examined CD163 expression (20) and found the ratio of $CD163^-$ to $CD163^+$ monocytes/macrophages to be significantly less in chemo/chemoradiation and greater with selicrelumab treatment, thus indicating "skewing" toward more M2-like with chemo/chemoradiation and reduction in M2-like skewing with selicrelumab therapy (**Fig. 3F**; Supplementary Fig. S3B).

Finally, we sought evidence for T-cell functionality by mIHC, as measured by expression of effector molecules (PD-1, granzyme B) or the proliferation marker Ki67. We observed statistically significant greater positivity of PD-1^+ cells among both $CD4^+$ and $CD8^+$ T-cell subsets in selicrelumab-treated tumors, indicative of recent activation (**Fig. 3G**). In $CD8^+$ T cells, this was concordant with greater granzyme B positivity, which approached statistical significance, and a statistically significant increase in $Ki67^+$ cells among $CD8^+$ T cells, indicative of cytotoxic activity and population expansion, central to effective antitumor T-cell responses.

Systemic inflammation and immune cell activation

To understand immune activation following treatment, we measured 42 cytokines in the serum at baseline and compared levels with those measured on protocol day 8, corresponding to 5 days after neoadjuvant selicrelumab. Pooling patients from arm I and II together, 15 cytokines exhibited a mean fold change greater than 1.0, with two—CCL22 and CXCL10—significantly upregulated (**Fig. 4A**; Supplementary Fig. S4A). CCL22 is upregulated during inflammation, secreted by DCs, and mediates crucial DC:Treg interactions. CXCL10 is secreted by several cell types in response to IFNγ and is a chemoattractant for myeloid cells, T cells, and dendritic cells. For 13 cytokines with a fold change below 1.0, CCL11 was significantly less than baseline and IL4 was less, approaching statistical significance (**Fig. 4B**; Supplementary Fig. S4B). CCL11 and IL4 are both soluble factors linked to myeloid accumulation and Th2 immunity. The remaining 14 analytes, including IFNγ and IL12p70, were unchanged with treatment at this time point.

To measure peripheral immune activation, PBMC cells from baseline and 5 days after selicrelumab (protocol day 8) were analyzed by mass cytometry across 64 parameters (Supplementary Fig. S4C and S4D). Myeloid and lymphoid subpopulations were resolved across a two-dimensional TSNE plot (**Fig. 5A** and **B**). For antigen-presenting cells, we examined B cells, monocytes, and DCs. B cells decreased as a percentage among total $CD45^+$ cells, without significant change in HLA-DR expression (**Fig. 5C**). $CD141^+$ DCs remained stable as a percentage of $CD45^+$ cells and significantly greater as a percentage among $CD11c^+$HLA-DR^+CD14^- cells and nearly reaching statistical significance for greater HLA-DR expression (**Fig. 5D**). The percentage of $CD163^-$ (M1-like) $CD11b^+$ $CD68^+$ myeloid cells was significantly greater after selicrelumab treatment, with no change in HLA-DR expression (**Fig. 5E**). On the other hand, $CD163^+$ (M2-like) cells $CD11b^+$ $CD68^+$ myeloid cells were significantly lower after treatment, with lower expression of HLA-DR (**Fig. 5F**).

To examine T-cell activation, we used mass cytometry to quantify activation, proliferation, and other markers on $CD4^+$ and $CD8^+$ effector T-cell populations displayed in the TSNE plot in **Fig. 6A**. For both T-cell subsets, statistically significant increases in expression of Lag3, PD-1, TIGIT, CCR7, CD28, granzyme K, and especially 2B4 were observed 5 days after selicrelumab (**Fig. 6B**). T-bet and especially Ki-67 also increased in both $CD4^+$ and $CD8^+$ effector T cells after treatment. Examples of patient-specific treatment-induced changes are illustrated in **Fig. 6C** and **D**. Finally, CyTOF analysis showed that the percentage of peripheral $FOXP3^+$ $CD4^+$ T regulatory cells (Treg) increased with treatment (**Fig. 6E**), although Treg density was not significantly altered in the TME as determined by mIHC (**Fig. 3F**).

Assessing T-cell clonality across treatment course with selicrelumab

TCR deep sequencing was performed on 15 surgical samples from the clinical trial as well as on peripheral blood T cells from those patients obtained at baseline and serially after surgery through the end of study. Using TCRβ sequencing of tumor samples, we observed an average of 17,803 unique TCR clones in the TME ("tumor clones"; median 7,652; range, 1,528–69,237; **Fig. 7A**). For each patient, we then gated on the set of tumor clones and quantified this population in peripheral blood at baseline (prior to neoadjuvant selicrelumab) and/or at multiple time points after surgery and during the adjuvant selicrelumab/chemotherapy phase of the study (starting at cycle 1 day 1 or "C1D1"). These selection criteria thus narrow in on tumor-associated T-cell clones that may have been enriched as a result of selicrelumab treatment during either the neoadjuvant or adjuvant setting. The mean number of post-surgical time points was 5.3 ± 2.7 (mean ± SD, median 4, range, 1–12; 3 patients did not have post-surgical blood samples; **Fig. 7A**). To assess the overlap of clones detected in the tumor site across the blood samples within each patient sample set, including baseline and post-surgery, we calculated the Jaccard coefficient for all tumor-associated clones at all time points (**Fig. 7B**). The Jaccard coefficient measures similarity between finite sample sets, defined as the size of the intersection divided by the size of the union of the sample sets such that a value of 1 means identical and 0 means no similarity. Tumor clones seen in blood exhibited more similarity across all time points than they did to their matched tumor clones found only in the tumor (**Fig. 7B**).

Pooling across the 15 patients examined, we found that 54.4% of all tumor clones were only ever identified in the tumor, not in blood (**Fig. 7C**). Of the 15 patients examined, 3 patients had no post-surgical blood samples for follow-up, and for the remaining 12 patients, we found that only 9.9% of tumor clones were identified in baseline blood and never again in blood after surgery. In contrast, 24.3% of tumor clones were found in at least one blood sample after surgery, and 20.3% of tumor-associated clones were only found in post-surgery blood. Tumor clones undetected in blood at baseline but evident after surgery may include new tumor-specific clones induced following therapy with selicrelumab. Notably, for total tumor clones found only after surgery, 10.1% were found in two or more blood samples from the same patient and 0.73% of such tumor clones were found in every post-surgery time point—up to 12 post-surgery samples in some patients. For patients with two or more post-surgical blood samples ($n = 11$), a mean of 159 tumor clones were found consistently in every post-surgery blood sample (±SD 399 clones, range, 6–1,350 clones). For each of these tumor clones that were detected in every post-surgical sample, we determined the maximum frequency and the time point at which the maximum was achieved. For all patients and all tumor clones detected in every post-surgical sample, the average maximum frequency in the blood was 62.5 templates (SEM ± 53.3, median 42, range, 9–147). The most common time points of maximal frequency were cycle 2 day 1 and cycle 3 day 1, with a range from cycle 1 day 15 to end of study.

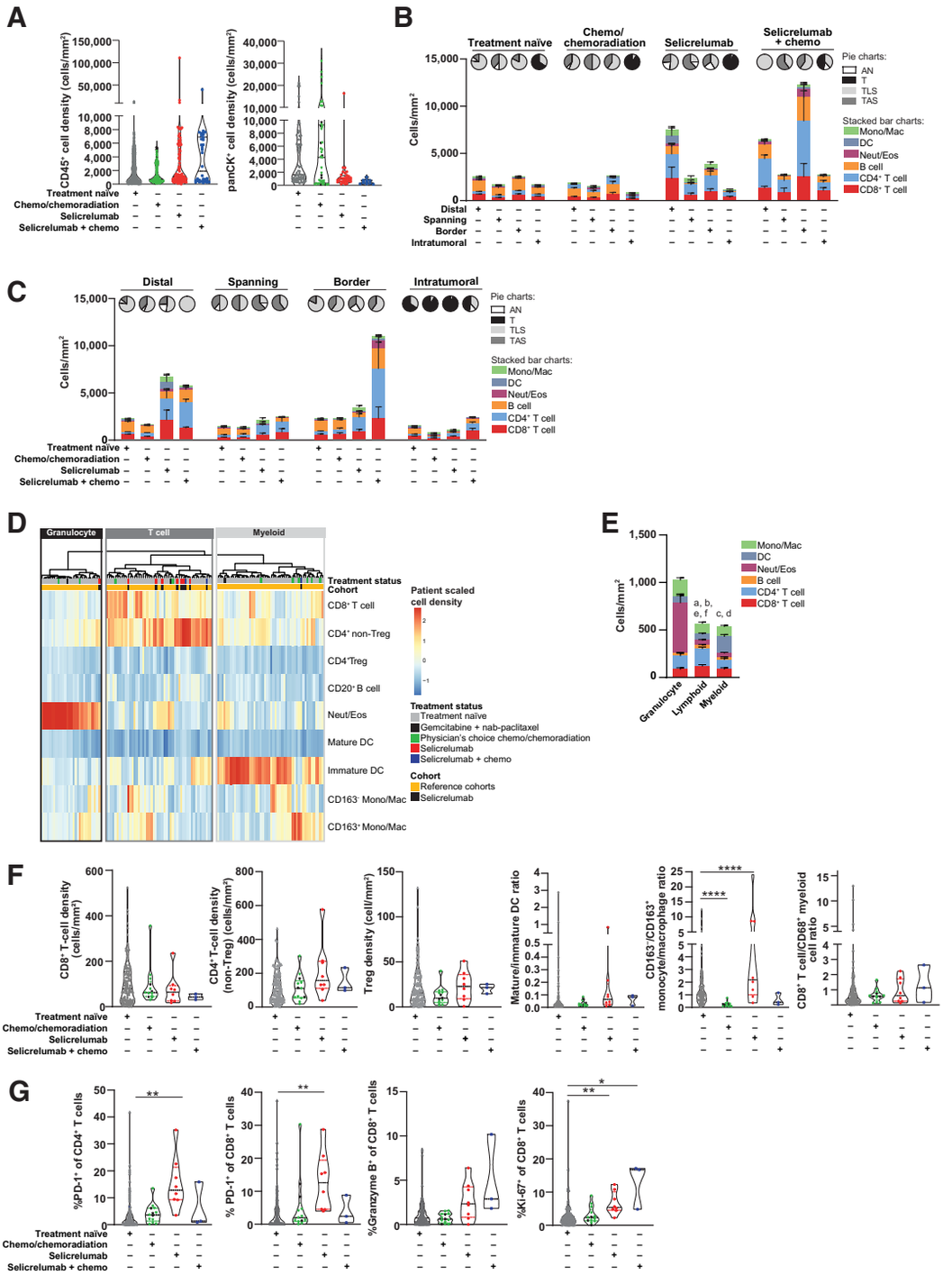

Figure 3.

Immune infiltrates in the TME of patients. **A,** Density of CD45$^+$ and pan cytokeratin$^+$ (PanCK) cells in the TME of four treatment groups. **B,** Broad immune composition in treatment groups by spatial location. **C,** Broad immune composition in spatial locations as a function of treatment groups. For **B** and **C**, contribution of histopathologic region type is displayed in pie graphs above each stacked bar. For **A–C**, each "N" is an ROI from a total of 20 patients for treatment naïve, 13 patients for chemo/chemoradiation, 8 patients for selicrelumab, and 3 patients for selicrelumab/chemotherapy. For **A** left (CD45), **B**, and **C**, included ROIs were tumor, tumor-associated stroma, normal-adjacent pancreas, and tertiary lymphoid structures, treatment naïve, $N = 295$ ROIs; chemo/chemoradiation, $N = 118$ ROIs; selicrelumab, $N = 87$ ROIs; selicrelumab/chemotherapy, $N = 33$ ROIs. For **A** right (PanCK$^+$), only tumor regions were analyzed: treatment naïve, $N = 61$ ROIs; chemo/chemoradiation, $N = 40$ ROIs; selicrelumab, $N = 32$ ROIs; selicrelumab/chemotherapy, $N = 10$ ROIs. Biostatistical comparisons for **A–C** are provided in Supplementary Table S3. (*Continued on the following page.*)

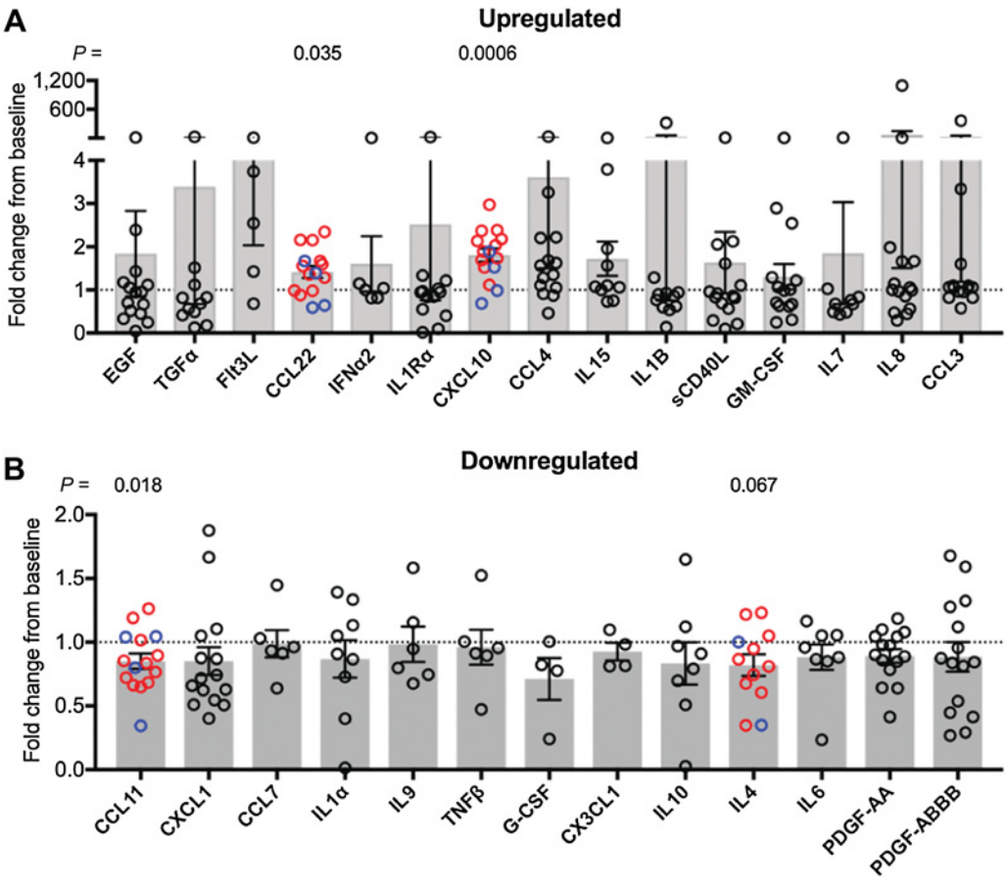

Figure 4.

Changes in serum cytokines between baseline and 5 days after selicrelumab. **A,** Upregulated or (**B**) downregulated fold changes in expression from baseline to 5 days after selicrelumab for each patient are displayed, in addition to mean ± SEM (gray bar and whisker plot), with dotted line indicating no change over baseline. For those with a statistically significant difference or a difference approaching significance, patient data points are color-coded (red, arm I; blue, arm II) with specific *P* values indicated as determined by Wilcoxon matched-pair signed rank test.

Discussion

Agonist CD40 mAbs are being pursued as a novel strategy for cancer immunotherapy based on the hypothesis from preclinical models that systemic CD40 activation activates cross-presenting DCs, reeducates tumor macrophages, and triggers antitumor T-cell immune responses (1). Corroborating data in patients treated with agonist CD40 mAb have been lacking. Here, we conducted a phase I clinical trial involving neoadjuvant and adjuvant CD40 mAb selicrelumab in patients with resectable PDAC and analyzed biosamples for evidence of treatment-induced modulation of the TME and systemic T-cell activation. Compared with untreated controls, surgical samples from patients receiving selicrelumab preoperatively exhibited less tumor fibrosis and greater likelihood of T-cell enrichment. Greater maturation of intratumoral DCs and fewer M2-like tumor-associated macrophages were also observed in selicrelumab-treated tumors than controls. In the periphery, increased activation and proliferation of $CD8^+$ and $CD4^+$ T cells and elevations of serum inflammatory cytokines were observed after selicrelumab treatment. Thus, consistent with mechanisms surmised from mouse models of pancreatic cancer but not previously demonstrated in humans, agonistic CD40 mAb alters the PDAC TME in patients, enhances T-cell infiltration and activation, and modulates inflammatory cytokines. These results suggest a novel

(*Continued.*) **D,** Unsupervised hierarchical clustering of histopathologically identified invasive tumor regions. Input was patient summarized data for cell density for various immune cell types; each patient is a column. Treatment status of chemo/chemoradiation patients is shown as both black and green, as indicated. **E**, Broad immune composition for the cluster types identified in **D**. "a" is **** comparison cluster T cell to myeloid for CD4; "b" is **** cluster T-cell to granulocyte for neutrophils/eosinophils (neut/eos); "c" is **** cluster myeloid to granulocytic for neut/eos; "d" is *** cluster myeloid to granulocytic for DCs, "e" is **** cluster T cell to myeloid for DCs, "f" is * cluster T cell to granulocyte for monocytes/macrophages. **F,** Density of $CD8^+$ T cells, $CD4^+$ T helper (non-Treg), $CD4^+$ T regulatory cells, and ratios of mature/immature DCs, $CD163^-/CD163^+$ monocytes/macrophages, and $CD8^+$ T cells/$CD68^+$ monocytes/macrophages. **G,** Percent cellular positivity for PD-1, granzyme B, and Ki67 on $CD4^+$ and $CD8^+$ T-cell subsets by treatment group. For **A**, **F**, **G**, patients who received gem + nab-paclitaxel in the neoadjuvant setting are colored black within the chemo/chemoradiation group, where all the other patients who received other chemo/chemoradiation combinations are green. For **D–G**, each "N" is a patient, $N = 104$ for treatment naïve, $N = 13$ for chemotherapy/chemoradiation, $N = 8$ for selicrelumab, $N = 3$ for selicrelumab/chemotherapy. For **F–G**, violin plots, all points are shown, lines at median and at 25th and 75th quartiles. Bar charts indicate mean ± SEM. Fisher exact test (2×3 contingency table) used to assess distributional differences (i.e., cluster skewing) among groups in **D**. For **F–G**, Kruskal–Wallis with Dunn multiple comparisons and correction. *, $P \le 0.05$; **, $P \le 0.01$; ***, $P \le 0.001$; ****, $P \le 0.0001$. Further experimental methods are provided in Supplementary Fig. S2 and Supplementary Table S4.

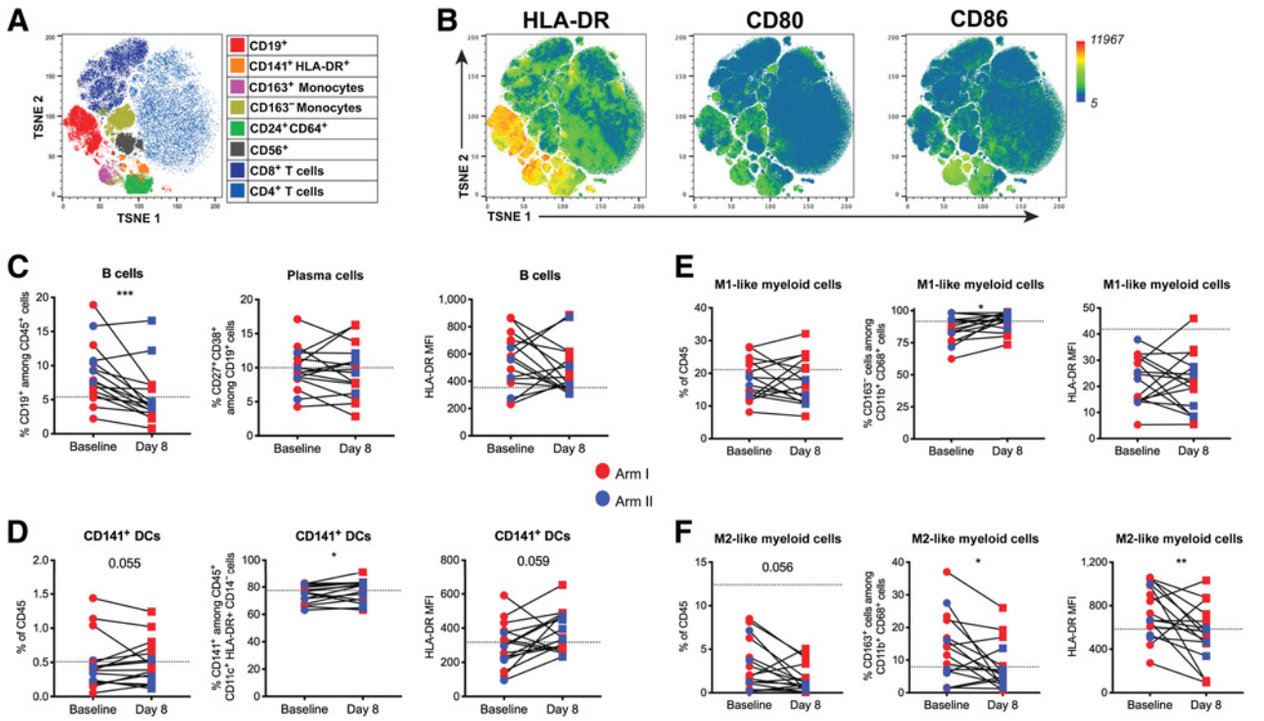

Figure 5.

CyTOF analysis of antigen-presenting cells in PBMC. **A,** TSNE plot displaying the major cell populations within the CD45$^+$ leukocyte population, gated as described in methods in Supplementary Fig. S4. **B,** Global MFI expression of MHC class II and costimulatory molecule expression. **C–F,** Changes in subsets or HLA-DR MFI expression for (**C**) B cells, (**D**) cDC1s, (**E**) M1-like myeloid cells, and (**F**) M2-like myeloid cells are shown. Red symbols indicate patients from arm I, blue indicates patients from arm II, circles denote baseline, squares indicate 5 days after selicrelumab (protocol day 8), and dotted line indicates mean values from normal donor controls. *, $P < 0.05$; **, $P < 0.01$; ***, $P < 0.001$, as determined by Wilcoxon matched-pair signed rank test.

mechanistic approach for immunotherapy of this and other tumors—potentially additive, not redundant, with checkpoint blockade.

A key to these findings was the application of a quantitative chromogen-based multiplexed IHC platform with computational image processing allowing simultaneous evaluation of 21 biomarkers in one FFPE tissue section (15, 16). In the recently published study by Liudahl and colleagues, in which the mIHC platform was applied to 104 resection samples from treatment-naïve PDAC patients, a reference atlas of subtypes of tumor immune microenvironments was constructed for this disease (12). With the ability to look across many ROIs in large surgical resections, the mIHC platform revealed intratumoral and intertumoral heterogeneity across a far wider area of the TME than is typically represented in small pieces of biopsy tissue. Importantly, this mIHC platform critically provides fine spatial information and addresses a limitation of single-cell analyses (21, 22).

By applying hierarchical clustering, we observed that 82% of PDAC tumors resected after selicrelumab were classified as T-cell–enriched, as compared with 36% T-cell–enriched tumors from treatment-naïve patients ($P = 0.004$) and 23% of such tumors in patients given only chemotherapy or chemoradiotherapy ($P = 0.012$). Thus, it was 2–3 times more likely for a selicrelumab-treated tumor to be T-cell–enriched than other tumors. Our findings indicate that a single dose of selicrelumab with or without chemotherapy converts T-cell–low PDAC tumors to T-cell–high (i.e., "cold" to "hot"). The conversion may be important because in mice, T-cell–high PDAC tumors are sensitive to CD40/checkpoint-based immunotherapy, whereas T-cell–low tumors are not (23). The greater PD-1-positivity observed on CD4$^+$ and CD8$^+$ T cells in the TME after selicrelumab implies potential further clinical synergy via PD-1-blockade.

Our data also provide evidence for systemic T-cell activation. In the 5 days after selicrelumab (protocol day 8), we observed increased markers of activation/exhaustion and proliferation of circulating CD8$^+$ and CD4$^+$ T cells. Although our analyses indicated robust pharmacodynamic effects on immune cells after selicrelumab treatment, it is possible that additional interventions may further potentiate the impact of agonistic CD40 therapy. Without a common or well-defined tumor antigen in PDAC to study, we utilized TCR deep sequencing to track T-cell clonal expansion and persistence. We focused on TCR clones identified in the resection sample (we called these "tumor clones") hypothesizing based on prior studies (24, 25) that this subpopulation might be enriched for tumor-specific T cells, at least as compared with whole peripheral blood. We were able to identify a small population of TCR clones, not detectable in the blood at baseline, but evident and persistent in the blood at multiple time points during adjuvant therapy. These findings are consistent with the hypothesis that selicrelumab (with or without chemotherapy) can drive expansion of new, clonal T-cell responses. These data are also consistent with TCR deep sequencing studies in transgenic mouse models of PDAC for which CD40 mAb, with or without gemcitabine/nab-paclitaxel (but not with chemotherapy alone) led to expansion of certain T-cell clones and recruitment of new populations of rare clones to the TME (4).

A key hypothesis underlying the mechanism of action of CD40 agonists is the activation and licensing of DCs, a cell increasingly

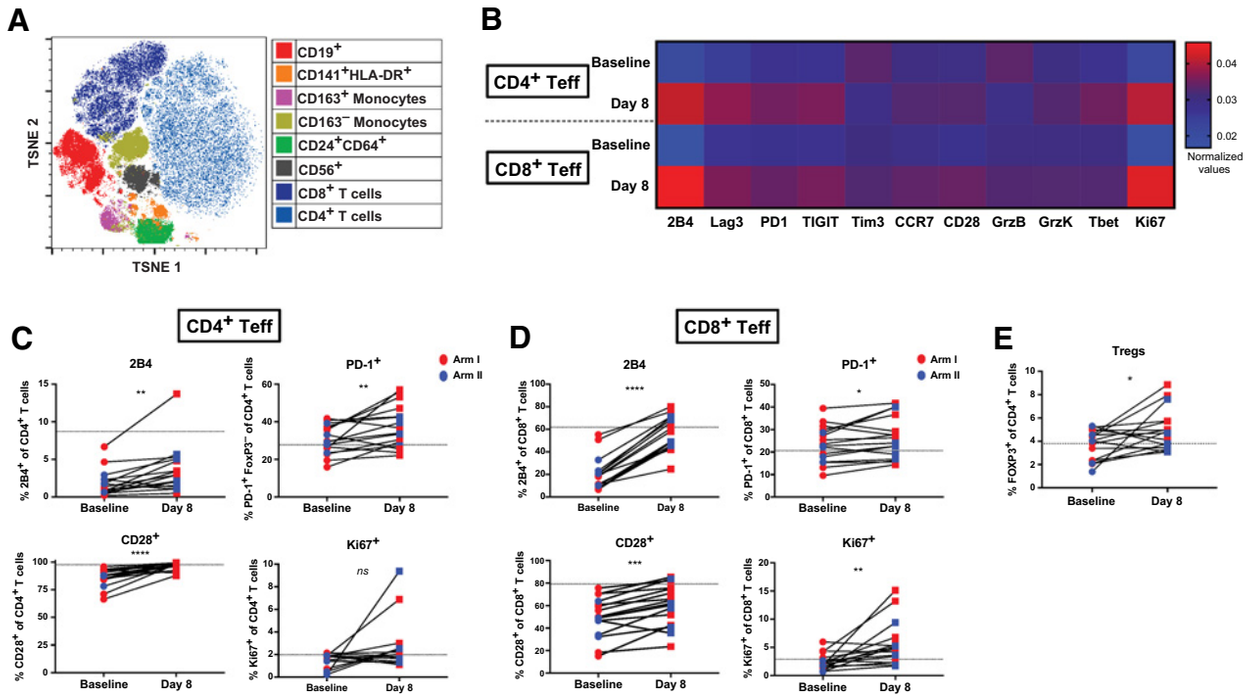

Figure 6.

CyTOF analysis of T cells in PBMC. **A,** TSNE plot displaying the major cell populations within the CD45$^+$ leukocyte population, gated as described in methods in Supplementary Fig. S4. **B,** Heat map displaying the normalized proportions of the indicated markers on CD4$^+$ effector T cells (CD4 Teff) or CD8$^+$ effector T cells (CD8 Teff) from baseline to 5 days after selicrelumab (protocol day 8). **C** and **D,** Plotted changes in highlighted markers for CD4$^+$ effector T cells (**C**) or CD8$^+$ effector T cells (**D**). **E,** Changes in the proportion of circulating Tregs. Red symbols indicate patients from arm I, blue indicates patients from arm II, circles denote baseline, squares indicate 5 days after selicrelumab (protocol day 8), and dotted line indicates mean values from normal donor controls. *, $P < 0.05$; **, $P < 0.01$; ***, $P < 0.001$; ****, $P < 0.0001$, as determined by Wilcoxon matched-pair signed rank test.

appreciated to be dysfunctional in cancer. In pancreatic cancer, in both mice and patients, DC dysfunction presents as an early, systemic, and progressive vulnerability—although this is clearly reversible *in vivo* in mouse models using CD40 mAb or CD40 mAb with Flt3 ligand (26, 27). DC dysfunction is not repaired with checkpoint therapy (targeting PD-1, PD-L1, or CTLA-4) alone. Here, we examined the rare DC population in the PDAC TME and found that density of mature DC was greater in the selicrelumab-treated tumors compared with either untreated tumors or chemo/chemoradiation-treated tumors. In intratumoral spatial locations, the ratio of mature/immature DCs was increased in both selicrelumab groups as compared with untreated or chemo/chemoradiation groups. In peripheral blood after selicrelumab, there was a greater percentage of CD141-expressing DCs that are critical in priming antitumor immunity (28). These DC exhibited a trend toward increased expression of HLA-DR. It is important to note that this study did not include procurement of any biosamples sooner than 5 days after selicrelumab, which is likely beyond the window of maximal pharmacodynamic response to CD40 mAb. Prior human and mice studies indicate the peak effect of CD40 mAb on APC is 24–72 hours after i.v. administration (4, 11, 19, 29). This likely also explains why certain cytokines such as IL12 were not found to be increased in the serum of patients 5 days after treatment with selicrelumab (protocol day 8), suggesting that earlier time points may better capture systemic cytokine release.

Monocyte/macrophages were also altered in patients treated with selicrelumab. Based on hierarchical clustering, 50 of all 128 tumor samples here were classified as myeloid-enriched based on the mIHC platform results; however, none of the selicrelumab tumors and only one of the selicrelumab/chemotherapy tumors fell within the category. Intratumorally, the ratio of CD163$^-$ to CD163$^+$ monocytes/macrophages was significantly greater in selicrelumab-treated tumors. In the periphery, CD163$^-$ (M1-like) CD11b$^+$ CD68$^+$ myeloid cells were increased after selicrelumab treatment, and CD163$^+$ (M2-like) cells CD11b$^+$ CD68$^+$ myeloid cells were significantly reduced after treatment, with lower expression of HLA-DR. These findings are consistent with reeducation away from an M2-like phenotype—and consistent with predictions from PDAC genetically engineered mice treated with CD40 mAb (3, 4).

We also observed less fibrosis and desmoplastic stroma in tumors treated with selicrelumab compared with untreated tumors, reproducing the phenotype observed in spontaneous KPC tumors after a single dose of agonist anti-mouse CD40 mAb (3, 4). This alteration in tumor stroma leads to transient tumor regressions in KPC mice, even in the absence of T cells, with a mechanism of action dependent on macrophage reeducation by CD40 activation and upregulation of metalloproteinases. Delivering chemotherapy 5 days after CD40 mAb in KPC mice—at a time of tumor stroma disruption—permits better chemotherapy delivery and subsequent tumor killing (30) and represents an important nonimmune mechanism of action of agonist CD40 mAb. In the adjuvant setting in the clinical trial here, chemotherapy was given 5 days after each dose of selicrelumab in part for this purpose. Whether fibrosis in PDAC patients after neoadjuvant therapy correlates with clinical outcome—and whether all "fibrosis" seen on resection samples reflects the same underlying biology—remains to be

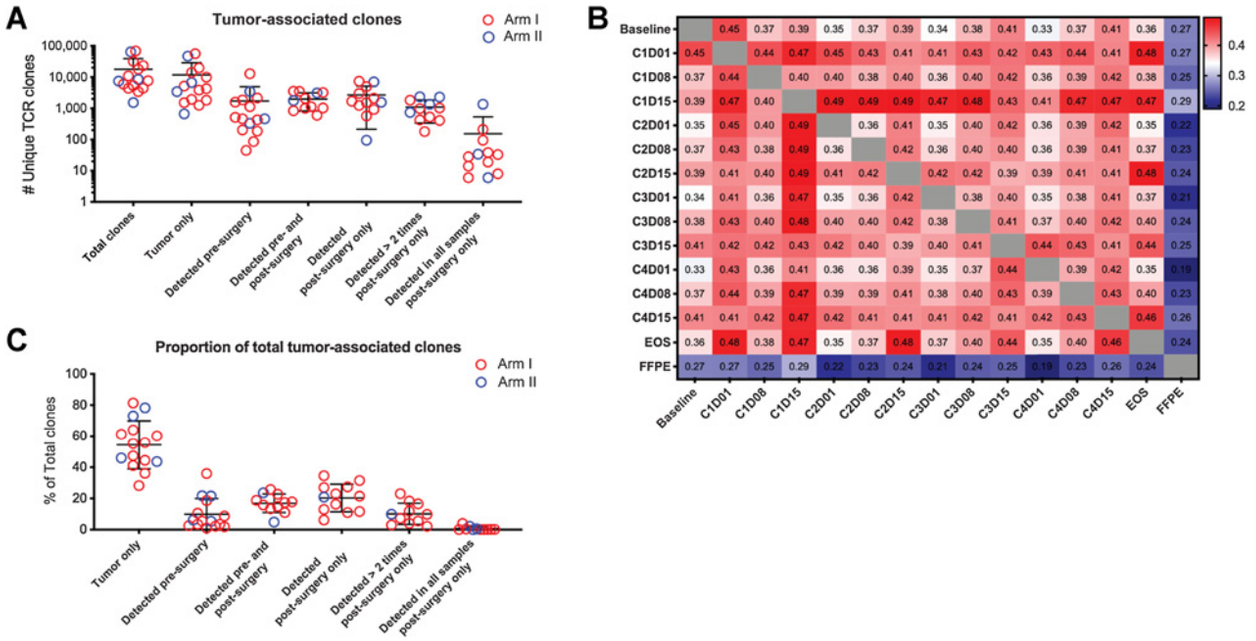

Figure 7.

TCR deep sequencing and analysis of tumor-associated clones. To enrich for tumor-associated T-cell clonotypes, all CDR3 amino acid TCR template reads were first gated on positive detection in the tumor site. **A,** Total tumor T-cell clones detected in tumor and blood, as indicated. All clones reported are detected in the tumor; "Tumor only" clones are never detected in any blood sample; "Detected pre-surgery" indicates tumor-associated clones preexisting at baseline before neoadjuvant selicrelumab administration; "Detected pre- and post-surgery" indicates tumor-associated clones detected in the baseline sample and any blood sample after surgery; all "Post-surgery only" columns indicate tumor-associated clones found only in the tumor and post-surgery samples, and not detected in the baseline blood sample. **B,** Jaccard coefficient matrix, comparing the frequencies of shared TCR CDR3 sequences as indicated. Protocol time points indicated by cycle number ("C") and day ("D") represent treatment days for the adjuvant selicrelumab/chemotherapy phase of the study. **C,** Frequency of tumor clones detected in each subset of time points as indicated, grouped as described in **A**. Each symbol represents a single patient, with horizontal line indicating mean, and error bars indicating SEM (**A** and **C**), or each box indicates the mean value across all patients at indicated time points (**B**). For **A** and **C**, red symbols indicate patients from arm I, and blue indicates patients from arm II.

determined. A recent paper, for example, shows that higher fibrosis after neoadjuvant chemoradiation therapy is associated with higher overall and DFS (31). The Erstad and colleagues study, however, focused exclusively on patients receiving FOLFIRINOX (31), whereas our study involved gemcitabine/nab-paclitaxel, limiting comparisons to this study.

Our results support strategies to incorporate CD40 activation into the armamentarium of cancer immunotherapy. Multiple agonist CD40 mAbs in addition to selicrelumab are under active clinical investigation, many of which differ in structure and function (1). Here, we report an acceptable safety profile, as expected from previous studies with this dose of selicrelumab given i.v. With the small sample size, it is difficult to compare DFS and OS to prior studies, although each is at least as good as historically documented for patients with R0 or R1 resections and adjuvant chemotherapy (32). It is encouraging that all patients on arm II remain alive between 12 and 18 months, although the sample size is small. We have used caution and avoided stating any correlations between clinical outcomes and biomarker data given the small number of patients. Pharmacodynamic assessments of treatment effects independent of clinical outcome, however, were robust, statistically significant and provide insights into mechanisms of action.

In comparison with other CD40 clinical trials, most notable are results from a phase Ib study (NCT03214250) with the agonist CD40 mAb sotigalimab—with gemcitabine and nab-paclitaxel, with or without nivolumab—that demonstrate clinical promise and an acceptable safety profile in patients with newly diagnosed metastatic PDAC. In this study (9), objective responses were documented in 14 of 24 DLT-evaluable patients [58%; 95% confidence interval (CI), 37–78). Median progression-free survival was 11.7 months (95% CI, 7.1–17.8) and median OS was 20.1 months (95% CI, 10.5–not estimable)—highly encouraging results compared with prior studies of gemcitabine/nab-paclitaxel alone. This approach is now being tested further in a national, randomized phase II clinical trial (NCT03214250).

In summary, using a neoadjuvant trial design and novel multiplexed tissue biomarker assays, we present the first evidence in humans that agonist CD40 mAb modulates the PDAC TME, decreases density of tumor stroma, activates DC, reeducates macrophages, and increases infiltration T cells with heighted activation and proliferation status. These changes in the TME are concomitant with observations of T-cell activation and clonal expansion in the periphery. As an immunotherapeutic approach distinct biologically and mechanistically from checkpoint blockade, CD40 activation addresses unmet challenges in cancer immunobiology and may provide novel, effective strategies for tumors relapsed or refractory to currently available immunotherapy.

Authors' Disclosures

K.T. Byrne reports grants from Parker Institute for Cancer Immunotherapy during the conduct of the study. D.L. Bajor reports grants from Seagen Inc, Rafael Pharmaceuticals, Calithera Biosciences, BMS, and Apexigen outside the submitted work. E.G. Chiorean reports grants from CITN during the conduct of the study, as

well as grants from Boehringer-Ingelheim, Roche-Ignyta, BMS, Celgene, Stemline, MacroGenics, Merck, Halozyme, Clovis, Fibrogen, Corcept, and Rafael, and personal fees from Celgene, Ipsen, Legend, Pfizer, Sobi, Bayer, Noxxon, and BioNTech outside the submitted work. M.H. O'Hara reports grants from Celldex, BMS, and Arcus; personal fees from Exelixis and Geneos; and grants and personal fees from Natera during the conduct of the study. S.A. Väyrynen reports grants from Finnish Cultural Foundation and Orion Research Foundation sr during the conduct of the study. J.C. Kaiser reports grants from Fred Hutchinson Cancer Research Center/Cancer Immunotherapy Trials Network during the conduct of the study. M. Stern reports personal fees from Roche during the conduct of the study. E.J. Wherry reports personal fees from Merck, Elstar, Janssen, Related Sciences, Synthekine, Surface Oncology, and Arsenal Biosciences outside the submitted work; in addition, E.J. Wherry has a patent on the PD-1 pathway issued. B.M. Wolpin reports grants and personal fees from Celgene, grants from Eli Lilly, and personal fees from Grail and BioLineRx outside the submitted work. E.M. Jaffee reports grants from SU2C during the conduct of the study, as well as grants from BMS and Lustgarten; personal fees from Genocea, Achilles, DragonFly, CSTONE, Parker Institute, and Candel; and grants and personal fees from AbMeta outside the submitted work. L.M. Coussens reports grants, personal fees, and other support from Cell Signaling Technologies and Syndax Pharmaceuticals; personal fees and other support from Verseau Therapeutics, Inc., Scientific Advisory Board, CytomX Therapeutics, Inc, Kineta Inc., Hibercell Inc., and Zymeworks, Inc.; other support from AstraZeneca Partner of Choice Network, OHSU site leader; personal fees from Koch Institute for Integrated Cancer Research, Massachusetts Inst. of Tech., Bloomberg-Kimmel Institute for Cancer Immunotherapy, Sidney Kimmel Comprehensive Cancer Center at Johns Hopkins: (2016–present; honorarium), Dana-Farber Cancer Center Breast SPORE, Dana-Farber/Harvard Cancer Center, University of California, San Diego Moores Cancer Center, Memorial Sloane Kettering Cancer Center; other support from Cancer Research Institute and The V Foundation for Cancer Research; personal fees and other support from Starr Cancer Consortium; personal fees from Lustgarten Foundation for Pancreatic Cancer Research, Therapeutics Working Group, NIH/NCI–Frederick National Laboratory Advisory Committee (FNLAC), AbbVie Inc, and Shasqi, Inc. during the conduct of the study, as well as personal fees and other support from Cell Signaling Technologies, Syndax Pharmaceuticals, and personal fees from Acerta Pharma, LLC, Innate Pharma, Carisma Therapeutics Inc, Verseau Therapeutics, Inc, CytomX Therapeutics, Inc., Kineta Inc, Hibercell, Inc, Zymeworks, Inc., Scientific Advisory Board, Koch Institute for Integrated Cancer Research, Massachusetts Inst. of Tech, Bloomberg-Kimmel Institute for Cancer Immunotherapy, Sidney Kimmel Comprehensive Cancer Center at Johns Hopkins, Dana-Farber Cancer Center Breast SPORE, Dana-Farber/Harvard Cancer Center, University of California, San Diego Moores Cancer, Memorial Sloane Kettering Cancer Center, Starr Cancer Consortium, Lustgarten Foundation for Pancreatic Cancer Research, Therapeutics Working Group, NIH/NCI-Frederick National Laboratory Advisory Committee (FNLAC), Susan G Komen Foundation, Komen Scholar, AbbVie Inc, and Shasqi, Inc outside the submitted work. R.H. Vonderheide reports personal fees from Medimmune and Verastem and grants from Fibrinogen, Janssen, and Lilly outside the submitted work; in addition, R.H. Vonderheide has patents for Universal Cancer Antigens issued, Cellular Therapy issued, licensed, and with royalties paid from Novartis, and research antibody with royalties paid from BD Biosciences. No disclosures were reported by the other authors.

Authors' Contributions

K.T. Byrne: Data curation, formal analysis, investigation, methodology, writing–original draft, writing–review and editing. **C.B. Betts:** Resources, data curation, formal analysis, investigation, visualization, methodology, writing–original draft, writing–review and editing. **R. Mick:** Conceptualization, formal analysis, investigation, visualization, methodology, writing–original draft, writing–review and editing. **S. Sivagnanam:** Resources, data curation, software, formal analysis, investigation, visualization, methodology, writing–original draft, writing–review and editing. **D.L. Bajor:** Conceptualization, resources, data curation, investigation, writing–review and editing. **D.A. Laheru:** Resources, data curation, investigation, writing–review and editing. **E.G. Chiorean:** Resources, data curation, investigation, writing–review and editing. **M.H. O'Hara:** Resources, data curation, investigation, writing–review and editing. **S.M. Liudahl:** Data curation, software, formal analysis, investigation, visualization, methodology, writing–review and editing. **C. Newcomb:** Data curation, formal analysis, visualization, writing–review and editing. **C. Alanio:** Formal analysis, investigation, methodology, writing–original draft, writing–review and editing. **A.P. Ferreira:** Resources, data curation, writing–review and editing. **B.S. Park:** Formal analysis, investigation, writing–original draft, writing–review and editing. **T. Ohtani:** Formal analysis, investigation, writing–review and editing. **A.P. Huffman:** Formal analysis, investigation, writing–review and editing. **S.A. Väyrynen:** Formal analysis, investigation, writing–review and editing. **A. Dias Costa:** Formal analysis, investigation, writing–review and editing. **J.C. Kaiser:** Data curation, investigation, project administration, writing–review and editing. **A.M. Lacroix:** Data curation, formal analysis, project administration, writing–review and editing. **C. Redlinger:** Data curation, investigation, project administration, writing–review and editing. **M. Stern:** Resources, investigation, writing–review and editing. **J.A. Nowak:** Resources, formal analysis, writing–review and editing. **E.J. Wherry:** Formal analysis, investigation, writing–review and editing. **M.A. Cheever:** Resources, supervision, writing–review and editing. **B.M. Wolpin:** Resources, formal analysis, supervision, investigation, writing–review and editing. **E.E. Furth:** Data curation, formal analysis, funding acquisition, investigation, writing–review and editing. **E.M. Jaffee:** Resources, funding acquisition, investigation, writing–review and editing. **L.M. Coussens:** Conceptualization, resources, formal analysis, supervision, funding acquisition, investigation, methodology, writing–original draft, writing–review and editing. **R.H. Vonderheide:** Conceptualization, resources, data curation, formal analysis, supervision, funding acquisition, validation, investigation, writing–original draft, project administration, writing–review and editing.

Acknowledgments

This work was supported by a Stand Up To Cancer–Lustgarten Foundation Pancreatic Cancer Convergence Dream Team Translational Research Grant (SU2C-AACR-DT14-14; to E.M. Jaffee, R.H. Vonderheide, L.M. Coussens), a Research Acceleration Network grant from the Pancreatic Cancer Action Network (to R.H. Vonderheide), the Lustgarten Foundation (to B.M. Wolpin), and the following grants from the NIH: P30 CA016520, R01 CA229803, and R01 CA169123 (to R.H. Vonderheide); U01 CA224012, U2C CA233280, R01 CA223150, R01 CA226909, and R21 HD099367 (to L.M. Coussens); and UM1 CA154967 (Cancer Immunology Trials Network; to M.A. Cheever). Stand Up to Cancer is a division of the Entertainment Industry Foundation. The indicated SU2C-LF grant is administered by the American Association for Cancer Research, the scientific partner of SU2C. Additional support is provided by the Parker Institute for Cancer Immunotherapy (to K.T. Byrne, C. Alanio, E.J. Wherry, R.H. Vonderheide), the Knight Cancer Institute (to L.M. Coussens), the Brenden-Colson Center for Pancreatic Care at OHSU (to L.M. Coussens), and the Hale Center for Pancreatic Cancer Research (to B.M. Wolpin). We thank the Cancer Immunotherapy Trials Network for help with protocol development and performance; Drs. Daniel Abbott, Dafna Bar-Sagi, Ronald DeMatteo, Doug Fearon, George Fisher, and Margaret Tempero for valuable discussions; and the Corporal Michael J. Crescenz VA Medical Center (Philadelphia, PA) for the use of the CyTOF Core Facility.

The publication costs of this article were defrayed in part by the payment of publication fees. Therefore, and solely to indicate this fact, this article is hereby marked "advertisement" in accordance with 18 USC section 1734.

Note

Supplementary data for this article are available at Clinical Cancer Research Online (http://clincancerres.aacrjournals.org/).

Received March 24, 2021; revised April 29, 2021; accepted May 28, 2021; published first June 10, 2021.

References

1. Vonderheide RH. CD40 agonist antibodies in cancer immunotherapy. Annu Rev Med 2020;71:47–58.
2. Vonderheide RH. The immune revolution: a case for priming, not checkpoint. Cancer Cell 2018;33:563–9.
3. Beatty GL, Chiorean EG, Fishman MP, Saboury B, Teitelbaum UR, Sun W, et al. CD40 agonists alter tumor stroma and show efficacy against pancreatic carcinoma in mice and humans. Science 2011;331:1612–6.
4. Byrne KT, Vonderheide RH. CD40 stimulation obviates innate sensors and drives T cell immunity in cancer. Cell Rep 2016;15:2719–32.
5. Morrison AH, Diamond MS, Hay CA, Byrne KT, Vonderheide RH. Sufficiency of CD40 activation and immune checkpoint blockade for T cell priming and tumor immunity. Proc Natl Acad Sci U S A 2020;117:8022–31.
6. Winograd R, Byrne KT, Evans RA, Odorizzi PM, Meyer AR, Bajor DL, et al. Induction of T-cell immunity overcomes complete resistance to PD-1 and

CTLA-4 blockade and improves survival in pancreatic carcinoma. Cancer Immunol Res 2015;3:399–411.
7. Rech AJ, Dada H, Kotzin JJ, Henao-Mejia J, Minn AJ, Twyman-Saint Victor C, et al. Radiotherapy and CD40 activation separately augment immunity to checkpoint blockade in cancer. Cancer Res 2018;78:4282–91.
8. Beatty GL, Torigian DA, Chiorean EG, Saboury B, Brothers A, Alavi A, et al. A phase I study of an agonist CD40 monoclonal antibody (CP-870,893) in combination with gemcitabine in patients with advanced pancreatic ductal adenocarcinoma. Clin Cancer Res 2013;19:6286–95.
9. O'Hara MH, O'Reilly EM, Varadhachary G, Wolff RA, Wainberg ZA, Ko AH, et al. An open-label, multicenter, phase 1b study evaluating the safety and efficacy of CD40 agonistic monoclonal antibody APX005M and chemotherapy, with or without nivolumab, for the treatment of metastatic pancreatic adenocarcinoma. Lancet Oncol 2021;22:118–31.
10. Gladue RP, Paradis T, Cole SH, Donovan C, Nelson R, Alpert R, et al. The CD40 agonist antibody CP-870,893 enhances dendritic cell and B-cell activity and promotes anti-tumor efficacy in SCID-hu mice. Cancer Immunol Immunother 2011;60:1009–17.
11. Vonderheide RH, Flaherty KT, Khalil M, Stumacher MS, Bajor DL, Hutnick NA, et al. Clinical activity and immune modulation in cancer patients treated with CP-870,893, a novel CD40 agonist monoclonal antibody. J Clin Oncol 2007;25:876–83.
12. Liudahl SM, Betts CB, Sivagnanam S, Morales-Oyarvide V, Yuan C, Hwang S, et al. Leukocyte heterogeneity in pancreatic ductal adenocarcinoma: phenotypic and spatial features associated with clinical outcome. Cancer Discov 2021; doi 10.1158/2159-8290.CD-20-0841.
13. Bankhead P, Loughrey MB, Fernandez JA, Dombrowski Y, McArt DG, Dunne PD, et al. QuPath: open source software for digital pathology image analysis. Sci Rep 2017;7:16878.
14. Tsujikawa T, Crocenzi T, Durham JN, Sugar EA, Wu AA, Onners B, et al. Evaluation of cyclophosphamide/GVAX pancreas followed by Listeria-Mesothelin (CRS-207) with or without nivolumab in patients with pancreatic cancer. Clin Cancer Res 2020;26:3578–88.
15. Tsujikawa T, Kumar S, Borkar RN, Azimi V, Thibault G, Chang YH, et al. Quantitative multiplex immunohistochemistry reveals myeloid-inflamed tumor-immune complexity associated with poor prognosis. Cell Rep 2017;19:203–17.
16. Tsujikawa T, Thibault G, Azimi V, Sivagnanam S, Banik G, Means C, et al. Robust cell detection and segmentation for image cytometry reveal Th17 cell heterogeneity. Cytometry A 2019;95:389–98.
17. Banik G, Betts CB, Liudahl SM, Sivagnanam S, Kawashima R, Cotechini T, et al. High-dimensional multiplexed immunohistochemical characterization of immune contexture in human cancers. Methods Enzymol 2020;635:1–20.
18. Nowak AK, Robinson BW, Lake RA. Synergy between chemotherapy and immunotherapy in the treatment of established murine solid tumors. Cancer Res 2003;63:4490–6.
19. Vonderheide RH, Burg JM, Mick R, Trosko JA, Li D, Shaik MN, et al. Phase I study of the CD40 agonist antibody CP-870,893 combined with carboplatin and paclitaxel in patients with advanced solid tumors. Oncoimmunology 2013;2:e23033.
20. Barros MH, Hauck F, Dreyer JH, Kempkes B, Niedobitek G. Macrophage polarisation: an immunohistochemical approach for identifying M1 and M2 macrophages. PLoS One 2013;8:e80908.
21. Elyada E, Bolisetty M, Laise P, Flynn WF, Courtois ET, Burkhart RA, et al. Cross-species single-cell analysis of pancreatic ductal adenocarcinoma reveals antigen-presenting cancer-associated fibroblasts. Cancer Discov 2019;9:1102–23.
22. Steele NG, Carpenter ES, Kemp SB, Sirihorachai VR, The S, Delrosario L, et al. Multimodal mapping of the tumor and peripheral blood immune landscape in human pancreatic cancer. Nature Cancer 2020;1:1097–112.
23. Li J, Byrne KT, Yan F, Yamazoe T, Chen Z, Baslan T, et al. Tumor cell-intrinsic factors underlie heterogeneity of immune cell infiltration and response to immunotherapy. Immunity 2018;49:178–93.
24. Bajor DL, Xu X, Torigian DA, Mick R, Garcia LR, Richman LP, et al. Immune activation and a 9-year ongoing complete remission following CD40 antibody therapy and metastasectomy in a patient with metastatic melanoma. Cancer Immunol Res 2014;2:1051–8.
25. Hopkins AC, Yarchoan M, Durham JN, Yusko EC, Rytlewski JA, Robins HS, et al. T cell receptor repertoire features associated with survival in immunotherapy-treated pancreatic ductal adenocarcinoma. Jci Insight 2018;3:e122092.
26. Lin JH, Huffman AP, Wattenberg MM, Walter DM, Carpenter EL, Feldser DM, et al. Type 1 conventional dendritic cells are systemically dysregulated early in pancreatic carcinogenesis. J Exp Med 2020;217:e20190673.
27. Hegde S, Krisnawan VE, Herzog BH, Zuo C, Breden MA, Knolhoff BL, et al. Dendritic cell paucity leads to dysfunctional immune surveillance in pancreatic cancer. Cancer Cell 2020;37:289–307.
28. Bottcher JP, Sousa CRE. The role of type 1 conventional dendritic cells in cancer immunity. Trends Cancer 2018;4:784–92.
29. Ruter J, Antonia SJ, Burris HA 3rd, Huhn RD, Vonderheide RH. Immune modulation with weekly dosing of an agonist CD40 antibody in a phase I study of patients with advanced solid tumors. Cancer Biol Ther 2010;10:983–93.
30. Long KB, Gladney WL, Tooker GM, Graham K, Fraietta JA, Beatty GL. IFN gamma and CCL2 cooperate to redirect tumor-infiltrating monocytes to degrade fibrosis and enhance chemotherapy efficacy in pancreatic carcinoma. Cancer Discov 2016;6:400–13.
31. Erstad DJ, Sojoodi M, Taylor MS, Jordan VC, Farrar CT, Axtell AL, et al. Fibrotic response to neoadjuvant therapy predicts survival in pancreatic cancer and is measurable with collagen-targeted molecular MRI. Clin Cancer Res 2020;26:5007–18.
32. Lewis R, Drebin JA, Callery MP, Fraker D, Kent TS, Gates J, et al. A contemporary analysis of survival for resected pancreatic ductal adenocarcinoma. HPB 2013;15:49–60.